Submillimetre observations of the two-component magnetic field in M82

Kate Pattle [ORCID],[1]★ Walter Gear [ORCID],[1] Matt Redman [ORCID],[1] Matthew W. L. Smith [ORCID][2] and Jane Greaves [ORCID][2]

[1]*Centre for Astronomy, Department of Physics, National University of Ireland Galway, University Road, Galway H91 TK33, Ireland*
[2]*School of Physics and Astronomy, Cardiff University, The Parade, Cardiff CF24 3AA, UK*

ABSTRACT

We observed the starburst galaxy M82 in 850 μm polarized light with the POL-2 polarimeter on the James Clerk Maxwell Telescope (JCMT). We interpret our observed polarization geometry as tracing a two-component magnetic field: a poloidal component aligned with the galactic 'superwind', extending to a height ∼350 pc above and below the central bar; and a spiral-arm-aligned, or possibly toroidal, component in the plane of the galaxy, which dominates the 850 μm polarized light distribution at galactocentric radii $\gtrsim$2 kpc. Comparison of our results with recent High-resolution Airborne Wideband Camera Plus (HAWC+) measurements of the field in the dust entrained by the M82 superwind suggests that the superwind breaks out from the central starburst at ∼350 pc above the plane of the galaxy.

Key words: galaxies: individual: M82 – galaxies: magnetic fields – submillimetre: galaxies.

1 INTRODUCTION

The magnetic fields observed in galaxies are thought to arise from the $\alpha\omega$-dynamo effect, in combination with a supernova-driven galactic wind (e.g. Beck et al. 1996). This dynamo results in spiral galaxies typically showing a magnetic field running parallel to their spiral arms, likely wound up over several Gyr (e.g. Jones et al. 2020), while magnetic field transport in galactic winds and outflows is thought to be a key mechanism by which the intergalactic medium is magnetized (e.g. Kronberg, Lesch & Hopp 1999). The dynamo mechanism has been shown to persist through periods of starburst activity, and to be enhanced by tidal interactions (Moss et al. 2014).

M82 is a nearby (3.5 Mpc; Jacobs et al. 2009) edge-on starburst galaxy, interacting with its neighbour M81. It has a bipolar 'superwind' emanating from its central region (e.g. Shopbell & Bland-Hawthorn 1998). M82 is classed as irregular, but none the less has a disc with a well-identified inclination angle of 76°.9 (Clark et al. 2018), and a 1-kpc-long bar (Telesco et al. 1991) from which weak $m = 1$ logarithmic spiral arms emanate (Mayya, Carrasco & Luna 2005).

The magnetic field of M82 is expected to consist of both a toroidal disc component and a poloidal wind component (e.g. Jones 2000). However, the brightness of the outflow-launching galactic nucleus, and the strength of the superwind, has made observing the planar component challenging (Jones et al. 2019).

M82 was first observed in extinction polarization by Elvius (1962), and was further observed in optical and 1.65 μm extinction polarization by Neininger, Beck & Backes (1990) and Jones (2000) respectively. These latter studies found a near-vertical field geometry in the galactic nucleus, inferred to trace the field in the superwind.

M82 was observed at 850 μm with SCUPOL on the James Clerk Maxwell Telescope (JCMT) by Greaves et al. (2000), who again

found a near-vertical field geometry in the galactic nucleus, but saw a broadly elliptical magnetic field geometry in the outer galaxy, which they interpreted as a magnetic bubble driven by the superwind. These data were reprocessed by Matthews et al. (2009), producing results consistent with those of Greaves et al. (2000), but in which the loop structure is less apparent.

M82 has been observed in radio polarization (6–22 cm) by Adebahr et al. (2017), who found a polarization geometry consistent with a planar field in the inner part of the galaxy, which they interpret as tracing a field running along the galactic bar.

The magnetic field in M82 has recently been observed with High-resolution Airborne Wideband Camera Plus (HAWC+) at 53 and 154 μm (Jones et al. 2019), finding that the near-vertical field geometry in the nucleus to extend into the galactic halo, inconsistent with the magnetic bubble model of Greaves et al. (2000). The magnetic field lines seen by HAWC+ have been inferred to be open – connecting the starburst core to the intergalactic medium, rather than creating a galactic fountain – in a recent preprint (Lopez-Rodriguez et al. 2021).

In this paper, we present 850 μm dust emission polarization observations of M82 made using the POL-2 polarimeter mounted on the Submillimetre Common User Bolometer Array-2 (SCUBA-2) camera on the JCMT. Section 2 describes the observations and the data reduction process. Section 3 describes our results. Section 4 compares our observations to previous measurements, and interprets our results. Our conclusions are presented in Section 5.

2 OBSERVATIONS

We observed M82 24 times between 2021 January 3 and 2021 January 29 using the POL-2 polarimeter on the SCUBA-2 camera (Holland et al. 2013) on the JCMT in Band 2 weather ($0.05 < \tau_{225\,\mathrm{GHz}} < 0.08$) under project code M20BP022. Each observation consisted of a 31-min POL-2-DAISY scan pattern.
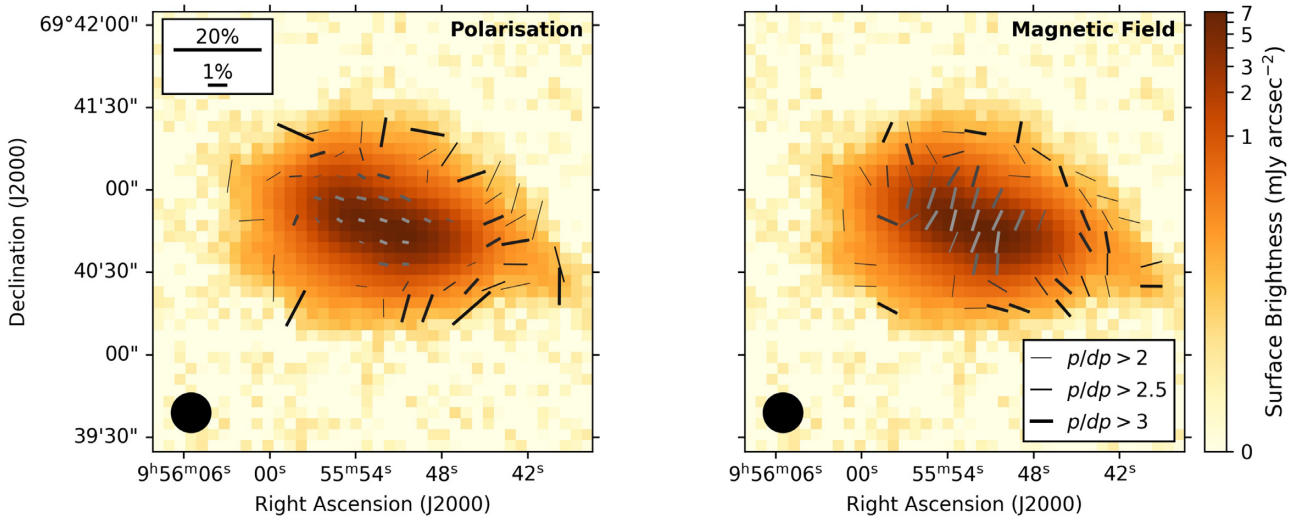
★ E-mail: katherine.pattle@nuigalway.ie

Figure 1. 850 μm POL-2 observations of M82. Left-hand panel: POL-2 polarization vectors, with length shown in square-root scaling for clarity. Right-hand panel: POL-2 *B*-field vectors (polarization vectors rotated by 90°), shown with uniform length. In both panels, the vectors are overlaid on 850 μm Stokes *I* emission. Vector thickness depends on signal-to-noise ratio in polarization fraction. Vector colour scaling is arbitrary and chosen for contrast against the background image.

The data were reduced using the *pol2map*[1] script recently added to the SMURF package in the STARLINK software suite (Chapin et al. 2013). See Pattle et al. (2021) for a detailed description of the current POL-2 data reduction process. Instrumental polarization (IP) was corrected for using the 'August 2019' IP model.[2] The 850 μm data were calibrated using a flux conversion factor (FCF) of 3159 mJy arcsec^{-2} pW^{-1}, the standard SCUBA-2 FCF of 2340 mJy arcsec^{-2} pW^{-1} (Dempsey et al. 2013) multiplied by a factor of 1.35 (Friberg et al. 2016).

We binned our output vector catalogue to 8-arcsec (approximately Nyquist-sampled) pixels. The per-pixel rms noise values in the vector catalogue were then remodelled using the *pol2noise* script, which models map variance as the sum of three components, based on exposure time, the presence of bright sources, and residuals. The average rms noise in Stokes *Q* and *U* in the centre of the map on 8-arcsec pixels is 0.0052 mJy arcsec^{-2} (1.2 mJy beam^{-1}).

The observed polarized intensity is given by

$$PI' = \sqrt{Q^2 + U^2}. \qquad (1)$$

However, this quantity is biased by its defined-positive nature. We debiased PI using the modified asymptotic estimator (Plaszczynski et al. 2014; Montier et al. 2015):

$$PI = PI' - \frac{1}{2}\frac{\sigma^2}{PI'}\left(1 - e^{-\left(\frac{PI'}{\sigma}\right)^2}\right), \qquad (2)$$

where σ^2 is the weighted mean of the variances σ_Q and σ_U,

$$\sigma^2 = \frac{Q^2\sigma_Q^2 + U^2\sigma_U^2}{Q^2 + U^2}, \qquad (3)$$

calculated on a pixel-by-pixel basis. Observed polarization fraction p' is then given by $p' = PI'/I$, and equivalently, debiased polarization fraction by $p = PI/I$. In the following analysis, we use p rather than p' except where specifically stated otherwise.

[1] http://starlink.eao.hawaii.edu/docs/sun258.htx/sun258ss73.html
[2] https://www.eaobservatory.org/jcmt/2019/08/new-ip-models-for-pol2-data/

Polarization angle is given by

$$\theta_p = 0.5\arctan(U, Q). \qquad (4)$$

Throughout this work we assume that dust grains are aligned with their minor axis parallel to the magnetic field direction (e.g. Andersson, Lazarian & Vaillancourt 2015), and so that the plane-of-sky magnetic field direction can be inferred by rotating θ_p by 90°. We discuss the validity of this assumption in Section 3.2, below. We note that the polarization angles that we detect are not true vectors, as they occupy a range in angle 0°–180°. We none the less refer to our measurements as vectors for convenience, in keeping with the general convention in the field.

3 RESULTS

The polarization vector maps observed with POL-2 are shown in Fig. 1. We show all vectors with $p/dp > 2$ and $I/dI > 10$. Vector weights in Fig. 1 show signal-to-noise ratio in p/dp. It can be seen that the position angles of the $p/dp > 2$ vectors agree well with those of the $p/dp > 3$ vectors, and so we include them in our analysis.

Our results agree well with both the original SCUPOL 850 μm vector map of Greaves et al. (2000), and the reprocessed map of Matthews et al. (2009). We note that the SCUBA/SCUPOL and SCUBA-2/POL-2 systems have nothing in common apart from the JCMT dish itself. The POL-2 and SCUPOL measurements were made using separate polarimeters, cameras, observing modes, and data reduction algorithms, and so are fully independent.

3.1 Magnetic field morphology

We see, broadly, two behaviours: in the galactic centre, the field is perpendicular to the direction of the bar, while in the outer galaxy, the field is parallel to the spiral arm structure.

The distribution of magnetic field angles is shown in Fig. 2. The field in the galactic centre can be seen as a strong peak at 161° ± 13° E of N (circular mean value, calculated over vectors where $I > 1.1$ mJy arcsec^{-2}), while the vectors associated with the outer galaxy
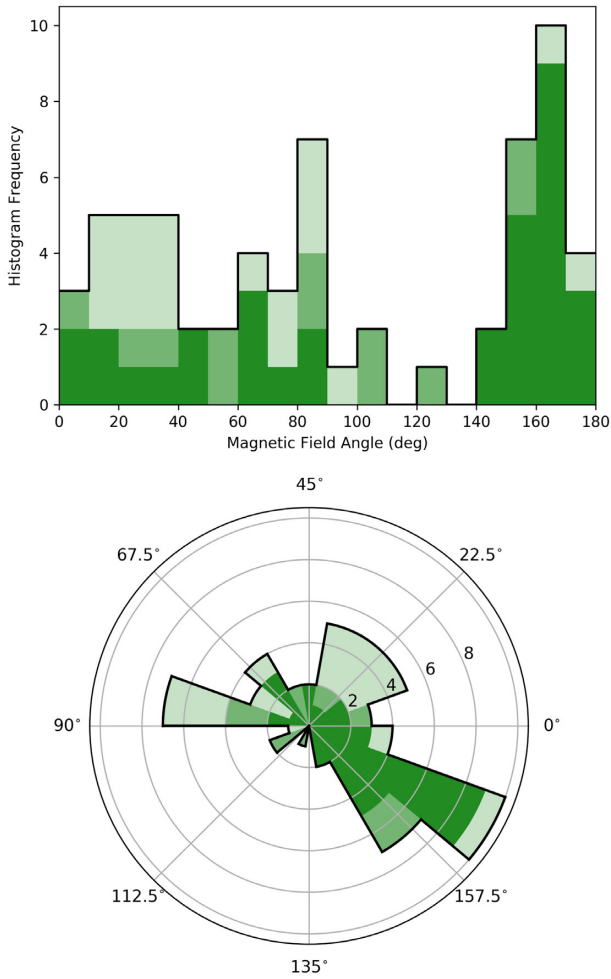
Figure 2. Histograms showing the distribution of magnetic field angles in M82. Top panel: conventional histogram. Bottom panel: circular histogram, showing the wrapping of magnetic field angle at 0°/180°. Shading denotes signal-to-noise ratio: dark green indicates vectors with $p/\mathrm{d}p > 3$; medium green, $p/\mathrm{d}p > 2.5$; light green, $p/\mathrm{d}p > 2$. Note the sharp peak at ∼161° indicating vectors tracing the poloidal field in the superwind.

occupy a broad range of angles, principally but not exclusively in the range ∼10–100° E of N.

We calculated the implied galactocentric radius of each pixel if it were tracing emission from the plane of the galaxy, assuming an inclination angle of 76°9 (Clark et al. 2018). Magnetic field angle as a function of implied galactocentric radius is shown in the central panel of Fig. 3, in which the two components of the angle distribution can be seen.

We adopted the spiral arm model of M82 proposed by Mayya et al. (2005), in which an $m = 1$ logarithmic spiral arm with a pitch angle of 14° extends from each end of the 60-arcsec-long bar, which is offset by 4° from the 26° position angle of the galaxy (Telesco et al. 1991). These spiral arms are overlaid on our data in the top panel of Fig. 3. It can be seen that the poloidal ∼161° field component extends ∼20 arcsec above and below the bar, but does not extend beyond the ends of the bar in the plane of the galaxy. Elsewhere, the field appears to be broadly toroidal around the galactic centre, or parallel to the spiral arm structure, as discussed below.

The offset between each magnetic field vector and the angle of the spiral arm component to which it is nearest is shown in the lower
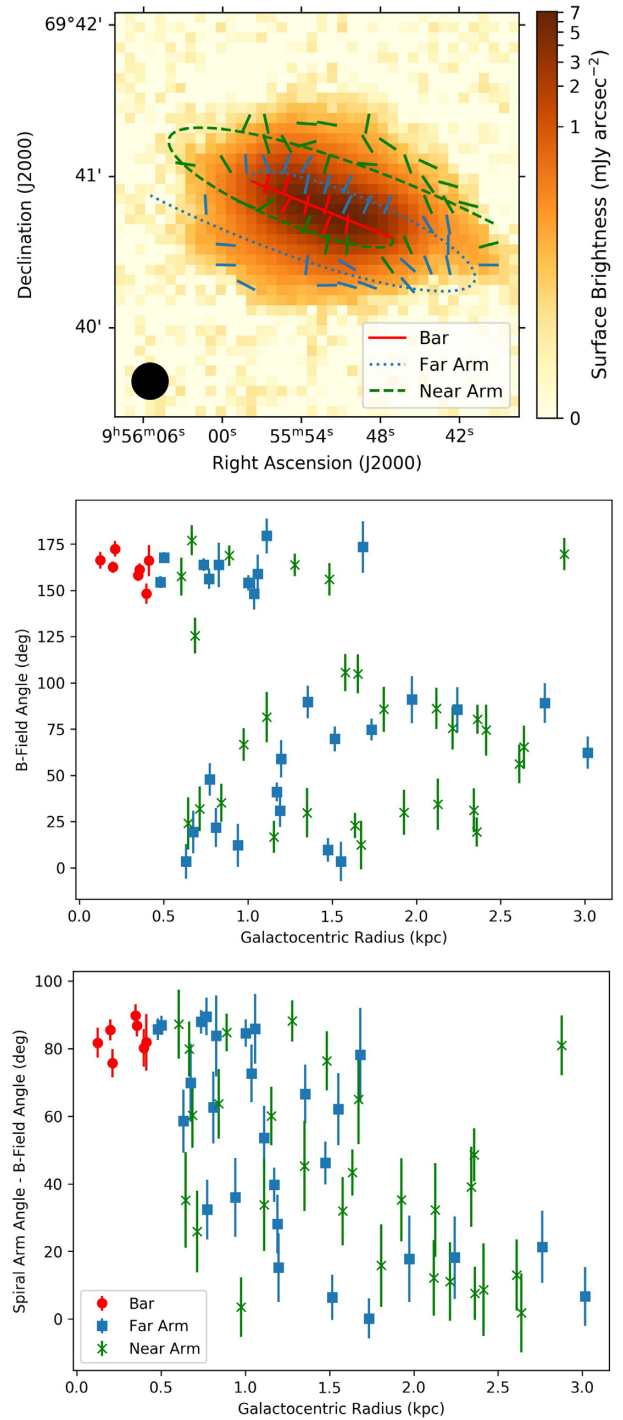

Figure 3. Comparison of magnetic field and spiral arm angles. Top panel: position of spiral arms (Mayya et al. 2005); vectors are colour coded by their nearest spiral arm. Middle panel: magnetic field angle as a function of implied galactocentric radius. Bottom panel: difference in angle between spiral arm structure and magnetic field as a function of implied galactocentric radius. The magnetic field appears to transition from being perpendicular to the bar in the galactic centre to being parallel to the spiral arms, or toroidal, at high galactocentric radius.

panel of Fig. 3. We can see the transition from a perpendicular, poloidal, field pattern that dominates in the galactic centre to a field approximately parallel to the spiral arms in the outer galaxy. With the exception of one data point at a radius of ∼3 kpc that is offset from the spiral arm direction by ∼80° (RA = 09ʰ55ᵐ49ˢ, Dec. = +69°41′20″.9), the spiral-arm-aligned component emanating from the disc appears to dominate over the poloidal component beyond a galactocentric radius ∼2 kpc. The transition occurs at an 850 μm flux density ∼0.6 mJy arcsec⁻², at a plane-of-sky distance ∼20 arcsec above/below the bar. Assuming an inclination of 76°.9 and a distance of 3.5 Mpc, this corresponds to a height above the disc of ∼350 pc.

3.2 Grain alignment

Observations of polarized dust emission typically show a power-law dependence, $p \propto I^{-\alpha}$, where $0 \leq \alpha \leq 1$ (Whittet et al. 2008; Jones et al. 2015). A steeper index (higher α) indicates either poorer grain alignment with respect to the magnetic field or more variation of the magnetic field direction along the line of sight (LOS): $\alpha = 0$ indicates that grains are consistently aligned throughout the LOS, while $\alpha = 1$ implies complete randomization of either grain alignment or magnetic field direction along the LOS (Pattle et al. 2019).

We measured α using the method described by Pattle et al. (2019), in which we assume that the underlying relationship between p and I can be parametrized as

$$p = p_{\sigma_{QU}} \left(\frac{I}{\sigma_{QU}} \right)^{-\alpha} , \qquad (5)$$

where $p_{\sigma_{QU}}$ is the polarization fraction at the rms noise level of the data σ_{QU}, and α is a power-law index in the range $0 \leq \alpha \leq 1$. We fitted the relationship between I and observed non-debiased polarization fraction p' with the mean of the Ricean distribution of observed values of p that would arise from equation (5) in the presence of Gaussian rms noise σ_{QU} in Stokes Q and U:

$$p'(I) = \sqrt{\frac{\pi}{2}} \left(\frac{I}{\sigma_{QU}} \right)^{-1} \mathcal{L}_{\frac{1}{2}} \left(-\frac{p_{\sigma_{QU}}^2}{2} \left(\frac{I}{\sigma_{QU}} \right)^{2(1-\alpha)} \right) , \qquad (6)$$

where $\mathcal{L}_{\frac{1}{2}}$ is a Laguerre polynomial of order $\frac{1}{2}$. See Pattle et al. (2019) for a derivation of this result. We restricted our data set to the central 3-arcmin diameter region over which exposure time, and so rms noise, is approximately constant (Friberg et al. 2016).

The relationship between p' and I in M82 is shown in Fig. 4. By fitting equation (6) to the data, we measure a best-fitting index of $\alpha = 0.25 \pm 0.08$. This suggests that in our observations of M82, grain alignment remains quite good and that a single average field direction along the LOS dominates the 850 μm emission at most locations, implying a sharp transition from the poloidal component to the orthogonal toroidal component dominating the emission profile above and below the bar. We see hints of a line of null polarization at ∼25 arcsec above and below the bar, perhaps delineating the locations where the wind and disc dust components contribute similar amounts of polarized 850 μm emission.

4 DISCUSSION

We posit that the polarization geometry observed at 850 μm can easily be reconciled with observations at other wavelengths if it traces the poloidal magnetic field in the central starburst at small galactocentric radii, and a toroidal/spiral-arm-aligned field in the disc of M82 at large galactocentric radii. In Fig. 3, we show that the magnetic field direction transitions from being broadly perpendicular
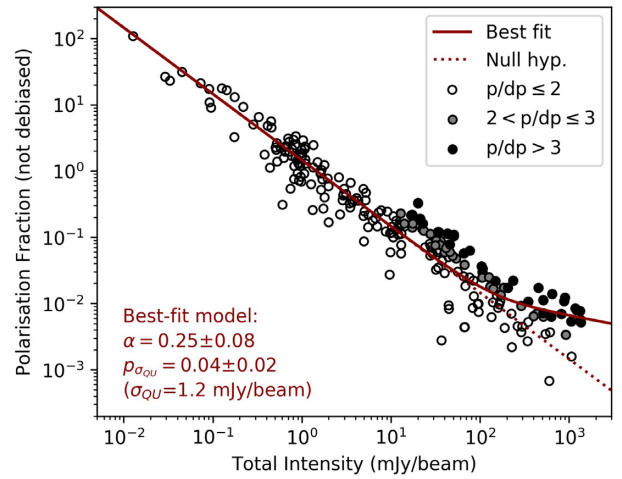

Figure 4. Non-debiased polarization fraction as a function of Stokes I intensity, fitted with a single-power-law distribution and a Ricean noise model, as described in the text. All data points in the central 3-arcmin-diameter region of the image are shown and fitted; those at $p/\mathrm{d}p > 2$ are shaded in grey; those at $p/\mathrm{d}p > 3$ are shaded in black. The best-fitting model, with a power-law index $\alpha = 0.25 \pm 0.08$, determined by fitting equation (6) to the data, is shown as a solid red line. The behaviour in the absence of true polarized signal, $p' = \sqrt{\pi/2}(I/\sigma_{QU})^{-1}$, is shown as a dashed red line.
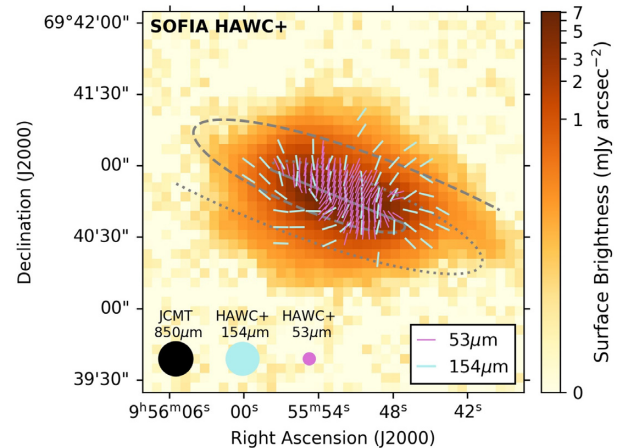

Figure 5. HAWC+ 53 μm (thin magenta) and 154 μm (thick light blue) magnetic field vectors (Jones et al. 2019), overlaid on 850 μm Stokes I emission. Mayya et al. (2005) spiral arm model is shown in light grey.

to the bar in the galactic centre to being broadly parallel to the spiral arms at larger galactocentric radii.

Many previous studies have suggested the existence of a two-component magnetic field in M82 (cf. Jones 2000, fig. 5). Observations of other spiral galaxies (e.g. M51; Jones et al. 2020) show magnetic fields running parallel to the spiral arms, in keeping with the $\alpha\omega$-dynamo model. We note that at the signal-to-noise ratio that we achieve in the outer parts of M82, it is difficult to definitively distinguish between a field generically toroidal around the galactic centre and one running along the spiral arms. However, both theory and previous observation lead us to expect fields to be parallel to spiral arms where such arms exist (Beck et al. 1996).

HAWC+ 53 and 154 μm vectors (Jones et al. 2019) are shown in Fig. 5. We see good agreement between the POL-2 and HAWC+ results in the centre of the galaxy, with all three wavelengths appearing to trace the poloidal field component. While the HAWC+ 53 μm

measurements do not extend far beyond the central bar, the 154 μm measurements extend considerably further. The POL-2 850 μm and HAWC+ 154 μm results agree at the ends of the bar, where we do not expect the outflow to be launching material. However, the two measurements disagree in the outer galaxy both above and below (particularly above) the galactic plane.

The fact that HAWC+ observations trace the galactic wind indicates that large amounts of dust are entrained in the galactic outflow (Jones et al. 2019). Based on their 53 μm observations, Jones et al. (2019) infer that the poloidal field geometry extends up to 350 pc above and below the plane, while the outflow itself extends at least 11 kpc from the plane (Devine & Bally 1999).

We see the poloidal field extending to ∼350 pc above and below the plane, in very good agreement with the extent over which the HAWC+ 53 μm emission is observed. However, the 154-μm-inferred field geometry continues to be poloidal to significantly larger distances above the plane, and the superwind field lines have been extrapolated to extend into the intergalactic medium (Lopez-Rodriguez et al. 2021). This suggests that at 850 μm, we are observing the poloidal magnetic field in the central starburst region. Beyond this region, our observations trace the magnetic field in the cold, high-column-density dust of the galactic plane, while 154 μm observations trace hot, low-column-density dust entrained in the superwind, in which the dust mass scale height is 1.4 ± 0.3 kpc (Leroy et al. 2015). The change in behaviour at ∼350 pc above the plane is consistent with models of M82 that call for the breakout from the starburst region to the beginning of the superwind to take place at around this vertical scale (e.g. Heckman, Armus & Miley 1990; Martini et al. 2018).

5 CONCLUSIONS

We have observed the starburst galaxy M82 in 850 μm polarized light using the POL-2 polarimeter on the JCMT. Our observations trace a poloidal magnetic field in the M82 central starburst region to heights ∼350 pc above the plane of the galaxy, but trace a field in the disc parallel to the spiral arms at galactocentric radii $\gtrsim 2$ kpc, in good agreement with predictions for a starbursting spiral galaxy. We see a significant discrepancy between POL-2 850 μm and HAWC+ 154 μm measurements in the outer galaxy, where the HAWC+ measurements trace hot, low-column-density dust entrained by the superwind. Observations across the submillimetre/far-infrared regime are thus necessary to disentangle the multiple magnetic field components of starburst galaxies.

ACKNOWLEDGEMENTS

DATA AVAILABILITY

REFERENCES

Adebahr B., Krause M., Klein U., Heald G., Dettmar R. J., 2017, A&A, 608, A29
Andersson B-G, Lazarian A., Vaillancourt J. E., 2015, ARA&A, 53, 501
Astropy Collaboration et al., 2013, A&A, 558, A33
Astropy Collaboration et al., 2018, AJ, 156, 123
Beck R., Brandenburg A., Moss D., Shukurov A., Sokoloff D., 1996, ARA&A, 34, 155
Chapin E. L., Berry D. S., Gibb A. G., Jenness T., Scott D., Tilanus R. P. J., Economou F., Holland W. S., 2013, MNRAS, 430, 2545
Clark C. J. R. et al., 2018, A&A, 609, A37
Dempsey J. T. et al., 2013, MNRAS, 430, 2534
Devine D., Bally J., 1999, ApJ, 510, 197
Elvius A., 1962, Lowell Obser. Bull., 5, 281
Friberg P., Bastien P., Berry D., Savini G., Graves S. F., Pattle K., 2016, in Holland W. S., Zmuidzinas J., eds, Proc. SPIE Vol. 9914, Millimeter, Submillimeter, and Far-Infrared Detectors and Instrumentation for Astronomy VIII. SPIE, Bellingham, p. 991403
Greaves J. S., Holland W. S., Jenness T., Hawarden T. G., 2000, Nature, 404, 732
Heckman T. M., Armus L., Miley G. K., 1990, ApJS, 74, 833
Holland W. S. et al., 2013, MNRAS, 430, 2513
Jacobs B. A., Rizzi L., Tully R. B., Shaya E. J., Makarov D. I., Makarova L., 2009, AJ, 138, 332
Jones T. J., 2000, AJ, 120, 2920
Jones T. J., Bagley M., Krejny M., Andersson B. G., Bastien P., 2015, AJ, 149, 31
Jones T. J. et al., 2019, ApJ, 870, L9
Jones T. J. et al., 2020, AJ, 160, 167
Kronberg P. P., Lesch H., Hopp U., 1999, ApJ, 511, 56
Leroy A. K. et al., 2015, ApJ, 814, 83
Lopez-Rodriguez E., Guerra J., Asgari-Targhi M., Schmelz J. T., 2021, ApJ, in press (arXiv:2102.03362)
Martini P., Leroy A. K., Mangum J. G., Bolatto A., Keating K. M., Sandstrom K., Walter F., 2018, ApJ, 856, 61
Matthews B. C., McPhee C. A., Fissel L. M., Curran R. L., 2009, ApJS, 182, 143
Mayya Y. D., Carrasco L., Luna A., 2005, ApJ, 628, L33
Montier L., Plaszczynski S., Levrier F., Tristram M., Alina D., Ristorcelli I., Bernard J. P., Guillet V., 2015, A&A, 574, A136
Moss D., Sokoloff D., Beck R., Krause M., 2014, A&A, 566, A40
Neininger N., Beck R., Backes F., 1990, in Beck R., Kronberg P. P., Wielebinski R., eds, Proc. IAU Symp. 140, Galactic and Intergalactic Magnetic Fields. Kluwer, Dordrecht, p. 253
Pattle K. et al., 2019, ApJ, 880, 27
Pattle K. et al., 2021, ApJ, 907, 88
Plaszczynski S., Montier L., Levrier F., Tristram M., 2014, MNRAS, 439, 4048
Shopbell P. L., Bland-Hawthorn J., 1998, ApJ, 493, 129
Telesco C. M., Campins H., Joy M., Dietz K., Decher R., 1991, ApJ, 369, 135
Whittet D. C. B., Hough J. H., Lazarian A., Hoang T., 2008, ApJ, 674, 304

This paper has been typeset from a T_EX/L^AT_EX file prepared by the author.